EXPERIMENTAL STUDY OF NONLINEAR VIBRATIONS OF THIN-WALLED CYLINDRICAL SHELLS

L. Gunawan[1)], R.J. Zwaan[2)], A.W.H. Klompé [2)]
[1)] ***Institut Teknologi Bandung, Indonesia***
[2)] ***Delft University of Technology, The Netherlands***

Keywords: *Stuctural dynamics, vibrations, nonlinear, experiments*

Abstract

Large amplitude vibration tests of thin-walled aluminum cylindrical shells were performed to validate results of theoretical analysis. The tests were carried out on four shells with practically clamped-clamped boundary conditions, two of them were perfect and the other two with built-in imperfections. The vibration behaviors of shell responses at large amplitudes of interest are the dependence of resonant frequency on the response levels and the possibility of response in the form of traveling waves. Parameters of the study were axial loads, geometric imperfections of the shell, excitation levels and direction of excitation frequency sweep. Comparison between the experimental and the theoretical results showed good agreements qualitatively.

1 Introduction

Cylindrical shells are widely applied in modern aircraft and space vehicle structures because of their high strength-to-weight ratio. The dynamic environment in which the vehicles usually operate may impose severe loads on the vehicle structure, especially at increased vehicle speeds. Under severe dynamic loads the cylindrical shell often vibrates at a large amplitude. This condition implies a nonlinear relationship between the displacement and the strain due to the curved geometry of the cylindrical shell.

This nonlinearity appears in two phenomena. Firstly, the resonant frequency becomes dependent on the amplitude of the vibration. Secondly, the response to dynamic forces may take the form of traveling waves although according to linear theory only a standing wave response is possible.

At the Delft University of Technology an intensive program is carried out in which buckling and vibrations of thin cylindrical shells under compressive loads and with imperfections are being studied by theoretical analysis. Despite the progress made, not many vibration experiments have been done as yet [8]. To validate the theoretical analysis of nonlinear vibrations of cylindrical shells [7,9], experiments on isotropic shell vibrations were carried out. This paper presents and discusses the results of the experiments and the comparison of the results with the calculated ones.

2 Analyses Review

2.1 The Governing Equations

Assuming that the radial displacement is positive inward (Fig.1) and introducing an Airy stress function F, related to the usual stress resultants by $N_x=F_{,yy}$, $N_y=F_{,xx}$ and $N_{xy}=-F_{,xy}$, the Donnel type non-linear imperfect cylindrical shell equations for an isotropic material are:

$$\frac{1}{Eh}\nabla^4 F = -\frac{1}{R}W_{,xx} - \frac{1}{2}L_{NL}\left(F, W+2\overline{W}\right) \qquad (1)$$

$$\frac{Eh^3}{12(1-\nu^2)}\nabla^4 W = -\frac{1}{R}F_{,xx} + L_{NL}\left(F, W+\overline{W}\right) + p - \bar{\rho}hW_{,tt} \qquad (2)$$

where $\overline{W}$ is the initial geometric imperfections, p is the excitation force per unit area, $\bar{\rho}$ is the specific mass, t denotes time, E is Young's modulus, ν is Poisson's ratio and ∇^4 is the two-dimensional biharmonic operator.

Under axial compressive load, W and F can be expressed as superpositions of two independent states of displacement and stress:

$$W = \tilde{W} + \hat{W} \qquad (3)$$

$$F = \tilde{F} + \hat{F} \qquad (4)$$

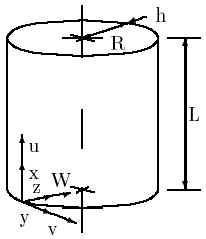

Symbol	Boundary Conditions			
SS3	$W=0$	$M_x=0$	$v=0$	$N_x=0$
C4	$W=0$	$W_{,x}=0$	$v=0$	$u=0$

Figure 1 Shell geometry, coordinate system and boundary conditions

where $\tilde{W}$ and $\tilde{F}$ are the static radial displacement and stress function of the static state while $\hat{W}$ and $\hat{F}$ are the displacement and the stress function of the dynamic state. By substituting Eq. 3 and 4 to Eq. 1 and 2, then equations governing the nonlinear static state and nonlinear dynamic state can be obtained [3].

2.2 Modeling of the Response

The analysis was carried out by introducing displacement functions in the governing equations.

$$\hat{W} = A(t)\, h \sin\frac{k\pi x}{L}\cos\frac{ly}{R} + B(t)\, h \sin\frac{k\pi x}{L}\sin\frac{ly}{R} + C(t)\, h \sin^2\frac{k\pi x}{L} \quad (5)$$

where k and l are respectively the axial half-waves and circumferential full waves numbers and h is the shell thickness.

This response function has two asymmetric modes, the driven mode with amplitude *A(t)* which is excited directly by the external excitation and the companion mode with amplitude *B(t)* which is excited by the driven mode at certain frequency range. These asymmetric modes are accompanied with an axisymmetric mode with amplitude *C(t)*.

2.3 Solution Methods

Two methods were available to solve the governing equations, the averaging method [9] and the numerical integration method [7]. In the first method the amplitudes of the axisymmetric modes is related to the asymmetric modes and the vibrations are assumed periodic. The averaging procedure is applied in solving the PDE's and the results are presented in the form of time-averaged vibration amplitudes. In the second method the axisymmetric mode remains as an independent coordinate. The PDE's is solved by using numerical integration in time. The response calculation of the second method provided a more direct comparison with experimental data as it could simulate both periodic and instationary vibrations.

Both methods essentially produced the same results [6]. Hence the validation was performed by using the second method.

3 Experiment

3.1 Test Setup

To verify the results of the numerical analysis, the conditions assumed must be realized in the test setup. Figure 2 shows the schematic view of the instrumentation. Two acoustic drivers provided acoustic waves which were projected at two circumferential places. Capacitive displacement transducers are used to measure the shell response. The contactless excitation and measurement systems were used to avoid disturbing changes of the vibration characteristics of the shells [2,6]. The parameters of the experiment were the excitation levels, the axial compressive loads, and the initial geometric imperfections.

3.2 Test Objects and Boundary Conditions

The test objects were four thin-walled cylindrical shells made by machining a seamless aluminum tube to specified dimensions. Two of the shells were perfect and the other two with axisymmetric imperfections. During test, each shell was clamped at both ends with end rings.

The wall thickness and the geometric imperfections of the shells were measured prior to the experiments. Table 1 shows the averaged wall thickness and the imperfections of the shells, which significantly characterize the shells [4,5]. The axial imperfections is modeled with the following form:

$$\overline{W} = \delta_1 \cos\frac{2\pi x}{L} \quad (6)$$

4. Small Amplitude Response Measurements

The mode shapes and the corresponding natural frequencies at small amplitude were needed to facilitate the choice of mode shapes to be considered in the large amplitude vibration tests. These were achieved by measuring the

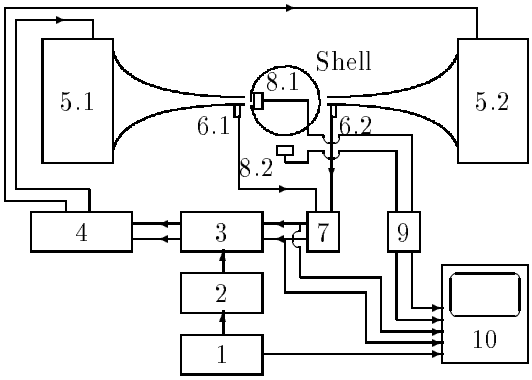

No	Description	No	Description
1	Generator Controller	6.1, 2	Microphone 1, 2
2	Wave Generator	7	Mic. Preamplifier
3	Exciter Synchronizer	8.1, 2	Displ. Transducer 1, 2
4	Power Amplifier	9	Signal Conditioner
5.1, 2	Acoustic Exciter 1, 2	10	FFT Analyzer

Figure 2 Schematic View of the Instrumentation

frequency response function (FRF) of the response with respect to the excitation.

4.1 Test Procedure

One acoustic driver was used to generate the small amplitude vibrations of the shell. The excitation signal was a fast sine sweep which was fed directly to the power amplifier and then to the acoustic driver. The frequency range of interest was between 400-1500 Hz which was divided into three smaller ranges, 400-800 Hz, 750-1150 Hz, and 1100-1500 Hz.

The FRF measurements were carried out at 51 points equally spaced over half the shell circumference at an axial position of 200 mm and 11 points in longitudinal direction. The 62 FRFs of each shell were curve-fitted simultaneously. Prior to the measurement, the linearity of the response was checked by comparing the FRFs of a point at three excitation levels.

4.2 Measurement Results

Figure 4 shows the FRFs of all shells in the frequency range between 400-800 Hz. The natural frequencies and the corresponding measured mode shapes are presented in Fig.5 as a plot between the natural frequencies and the number of circumferential waves *l*. Results of shell Liuip02 were not plotted because they are almost the same as those of Liuip01. In Fig.5 the measured natural frequencies are compared to their analytical counterparts calculated for

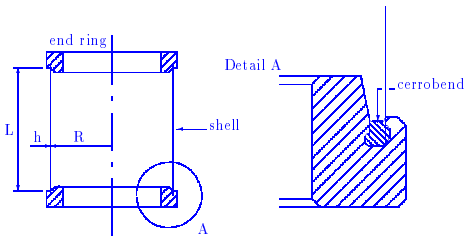

Figure 3 Sectional view of the shell clamped with

Shell	Wall thickness (h in mm)	Imperfections (δ_i)
Liupf01	0.253	-0.04
Liupf02	0.267	-0.01
Liuip01	0.273	-0.34
Liuip02	0.277	-0.34

Table 1 Shell dimensions and imperfections amplitude

shells with the same nominal geometry with SS3-SS3 and C4-C4 boundary conditions.

4.3 Factors Affecting the Measured Natural Frequencies

The influence of several parameters to the measured natural frequencies were tried to be kept as constant as possible. The measurements were performed at almost the same ambient temperature, 20°C. The clamping conditions appeared to be consistent as repeatable natural frequencies were measured when the shell was several times assembled to the end rings [6].

4.4 Small Amplitude Characteristics of the Shells

From the results of the measurement at small amplitude levels presented in Fig.5, some observation were taken:

The lowest natural frequency of each shell does not correspond to a mode with the lowest wave number, as commonly found in the case of a beam structure. This is explained in Ref.[10].

The real boundary conditions are closest to a C4-C4 condition.

The effect of wall thickness can be observed by comparing the results of shell Liupf01 to those of Liupf02. For low *l* values they are almost the same but for high *l* they have significant difference. This is in agreement the explanation given in Ref.[10, 11].

The influence of axisymmetric imperfections can be observed by comparing the results for shell Liupf02 and Liuip01. At low *l* values

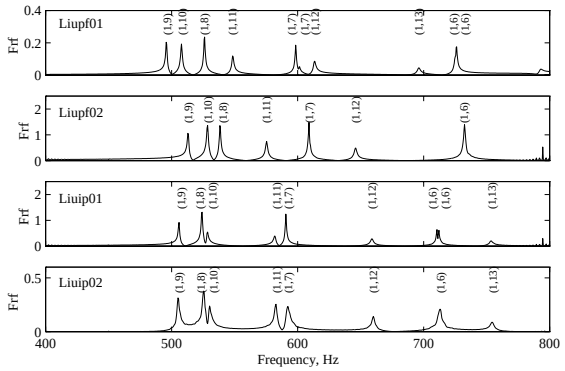

Figure 4 FRF of all four shells between 400--800 Hz with values (k,n) between parentheses

the frequencies of shell Liuip01 are slightly lower than those of shell Liupf02. This is in agreement with Ref.[9] which suggested that the axisymmetric imperfections, up to a certain amplitude, reduce the natural frequencies. At high *l* values the natural frequencies of Liuip01 are larger than those of Liupf02 since the wall thickness of shell Liuip01 is slightly thicker than that of shell Liupf02.

4.5 Vibration Modes for the Large Amplitude Test

The choice of vibration modes which would be suitable for the large amplitude vibration tests was based on the principal requirement of sufficient frequency separation of these modes from the frequencies of their neighboring modes. The adequate power of the excitation forces to obtain nonlinear vibration conditions was also considered which limited the choice to vibration modes with low axial half-wave number. Another requirement taken into account was the absence of any spatial preference of the vibration modes which have been observed for several modes. The best candidates for the large amplitude tests were:

- Mode (1,11) for shell Liupf01 and Liupf02.
- Mode (1,9) for shell Liuip01 and Liuip02.

5. Large Amplitude Response Measurements

5.1 Excitation Points

To obtain large response levels, two exciters were used as shown in Fig.2. They were placed opposite to each other while their excitation forces were controlled to be out of phase as the

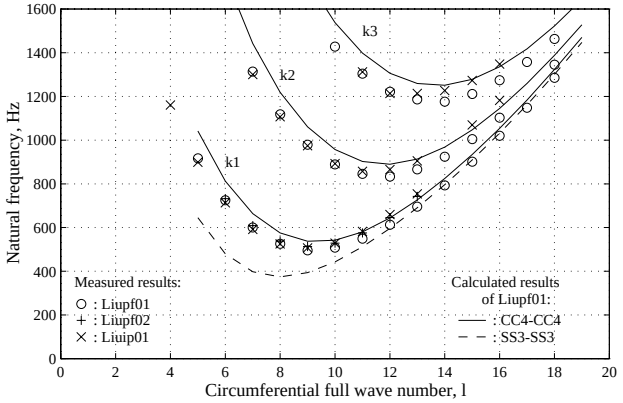

Figure 5 Natural freqs. vs circumferential wave number

modes of interest have odd number of circumferential waves.

5.2 Observation Points

The two displacement transducers were used to measure the driven and companion mode simultaneously. One transducer was positioned inside the shell exactly opposite to acoustic driver no.1 to measure the driven mode, as at that place always the antinode of the driven mode could be expected. The other one was placed at the node of the driven mode to measure the companion mode [2].

5.3 Test Procedure and Data Processing

In the vibration measurements stepped sine excitation forces were applied. To generate them, the wave generator supplied harmonic signals with a frequency sweep which varied from low to high values or vice versa. At preset frequencies the generator interrupted the sweep for a certain period and simultaneously sent a pulse signal to the FFT Analyzer. The analyzer after a certain time delay made records of the pressure and the response signals. This ensured that the shell reached steady state vibrations.

At each preset frequency the signals from the two microphones and the capacitive transducers were recorded and transformed into the frequency domain. Hence, at the end of the measurement $4\times N$ FFT spectra were obtained, N being the number of excitation frequencies. In reducing the data first a database was assembled that would facilitate further processing. This included for each group of N spectra the selection of pressure or displacement harmonics with the same frequency as the excitation

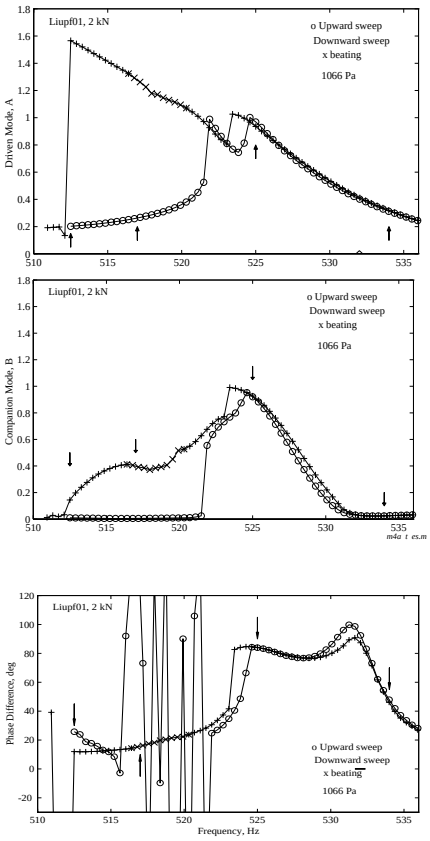

Figure 6 Measured response of mode (1,11) of shell Liupf01 for excitation pressure 1066 Pa with axial load 2 kN, a) driven mode, b) companion mode and c) phase difference. Conditions with arrow refer to Fig.7

frequency. The results were the first harmonic amplitudes of the pressures or the responses for each excitation frequency.

The measurement of response distributions was performed at each frequency of interest. At that frequency both transducer signals were recorded, the signal of transducer no.2 being recorded at several circumferential positions, and transformed into the frequency domain. At the end of the measurement $2\times N$ spectra were obtained, N being the number of positions of transducer no.2. The data reduction was carried out as explained previously, except that the selection was now made of displacement harmonics with the same frequency as the excitation frequency which was constant. At some measurement results, the contractive motion was identified by selecting the amplitude with frequency of twice the excitation frequency.

The nonlinear vibration tests were performed on the four shells for several axial loads. For each axial load the responses at several excitation levels were measured.

5.4.1 Vibrations of Perfect Shells

Basic behavior

The response characteristics of shell Liupf01 for mode (1,11) for an excitation pressure of 1066 Pa and axial load of 2 kN are considered here as a generic case. The characteristics are shown in Fig.6 in which (a) is the driven mode, (b) is the companion mode response and (c) is their phase difference. Both the responses for the upward and downward frequency sweeps are indicated. A softening behavior was found. A jump up at a frequency of 522 Hz occurred during the upward sweep, which was accompanied with a jump of the companion mode from zero, thus transforming the single mode response into a coupled mode response. After a further increase of the excitation frequency another jump occurred for both modes although not as large as before. The phase difference between the companion and the driven mode which was about 30 deg at the first jump gradually shifted to larger values and at the second jump the phase jumped to about 90 deg.

A further increase of the excitation frequency reduced the response and at 531 Hz the companion mode practically disappeared. The downward sweep response followed the same path as the upward sweep response until at 523 Hz a small jump down occurred slightly left of the secondary jump up. This jump down was also accompanied by the phase jump from almost 90 deg to 40 deg. Decreasing the excitation frequency further increased the level of the driven mode response but decreased the level of the companion mode response. The phase difference gradually decreased. Between 520 to 515 Hz a beating of the response occurred as shown in Fig.6. The beating was such that when the driven mode was in its maximum the companion mode was in its minimum. Below 515 Hz the driven mode still increased while the companion mode decreased. At 512 Hz the driven mode jumped down to a single mode response, accompanied by the sudden vanishing of the companion mode. The

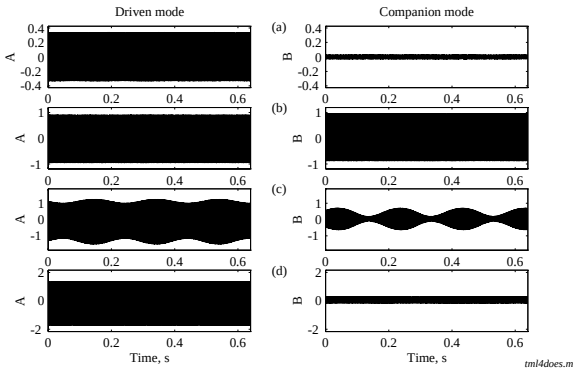

Figure 7 Time history of the response of mode (1,11) for excitation pressure 1066~Pa with axial load 2~kN during downward sweep for driven mode (left) and companion mode (right) at (a)~534~Hz, (b)~525~Hz, (c)~517~Hz and (d)~512.5~Hz

downward sweep responses between 515 and 512 Hz were conditionally stable as a slight disturbance to the shell could make the responses to jump to the single mode response.

Figure 7 shows the time responses of the driven and the companion mode recorded during the downward sweep at 534 Hz (a), 525 Hz (b), 517 Hz (c) and 512.5 Hz (d). Above the (linear) resonant frequency which was about 531 Hz, a steady state single mode response occurs. Slightly below the natural frequency the companion mode participates in a steady state coupled mode response. Below the small jump the companion mode decreases with decreasing frequency. In this region a nonstationary responses in the form of beating was observed. The phase and amplitude relation between the driven and the companion mode can be seen in Lissajous figures of the driven vs the companion mode, Fig.8. The plots indicate that the phase difference is not exactly 90 deg and that higher harmonics exist in the response. At 525 Hz a more or less circular response is shown, i.e. the driven and companion mode have almost equal amplitudes. Below the small jump, 517 Hz, the response is highly nonstationary due to beating. To analyze the beating, the response between 0.15 s to 0.244 s was selected, which shows the driven mode changing from a maximum to a minimum and the companion mode from minimum to maximum. The Lissajous plots of four smaller intervals were made, as shown in Fig.9. It can be seen that the beating response

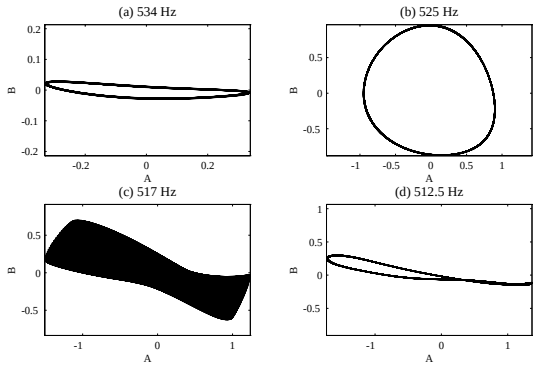

Figure 8 Lissajous figure of the driven and the companion mode at a) 534 Hz, b) 525 Hz, c) 517 Hz and d) 512.5 Hz

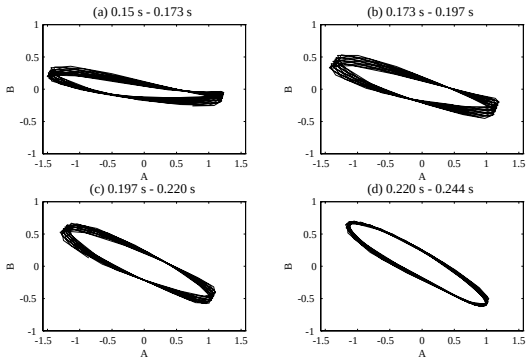

Figure 9 Lissajous figure of the driven and the companion mode at 517 Hz between a) 0.150 s – 0.173 s, b) 0.173 s – 0.197 s, c) 0.197 s – 0.220 s and d) 0.220 s – 0.244 s

indicates a regular change of single to coupled mode response. This was also suggested by Ref. [1].

Figure 6 also shows that the slope of the driven mode response curve does not show a distinct change when the response changes from a single mode to a coupled mode response during an upward or downward sweep near 531 Hz. This means that no pronounced bifurcation point was observed there, whereas Ref.[9] predicted a distinct bifurcation point.

Further, the time phase difference between the driven and companion mode varied from about 0 to 90 deg during an upward sweep excitation and vice versa. This is in agreement with the assumption taken in Ref.[9] that the phase difference does not need to be 90 deg. The varying phase difference between the driven and companion modes implies that the companion mode response can be split up into a part being in phase and a part with 90 deg phase difference with the driven mode. Consequently the part of the companion mode which is in

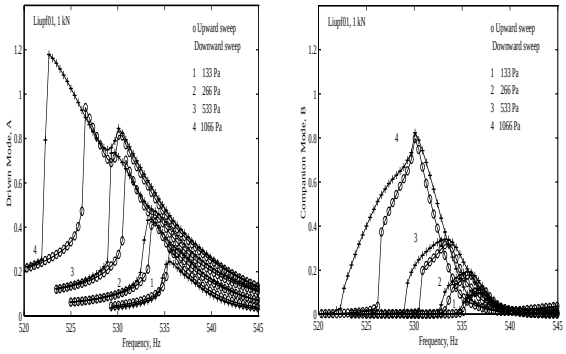

Figure 10 Response of shell Liupf01 with 1 kN axial load

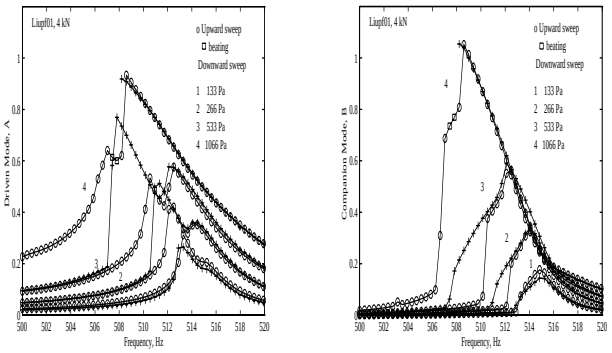

Figure 12 Response of shell Liupf01 with 4 kN axial load

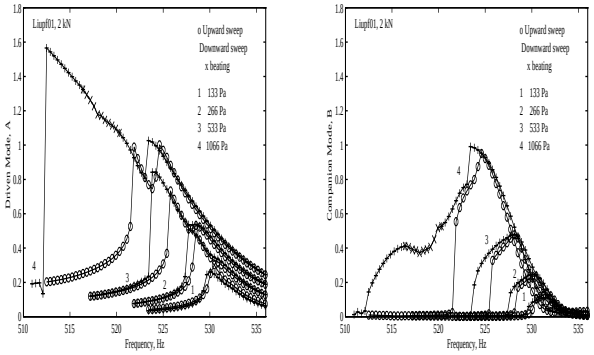

Figure 11 Response of shell Liupf01 with 2 kN axial load

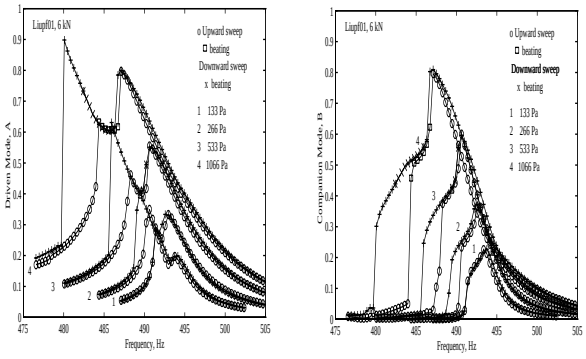

Figure 13 Response of shell Liupf01 with 6 kN axial load

phase with the driven mode enforces a circumferential drift of the response, implying that the maximum of the response is not at the excitation point. The part of the companion mode which has a time phase difference of 90 deg causes a response in the form of a traveling wave.

Influence of Excitation Levels and Axial Loads

The measurements with shell Liupf01 for mode (1,11) were carried out for four axial load values and at each axial load for four excitation levels. The results are shown in Figs.10 to 13. The followings are observed:

- The driven mode response curves show that the nonlinearity at a response level of 1.5 times the wall thickness is of a softening type.
- Higher response levels (due to higher excitation forces) widen the frequency range of the coupled mode response. For each axial load case the upper frequency limit of the range is not significantly altered and the lower frequency limit shifts to a lower frequency as the response level increases.
- Higher response levels also make the jump phenomenon and the peak of the coupled mode response to become more pronounced.
- By comparing Figs.10 to 13 it can be observed that the axial load reduces the natural frequency of the shell but do not significantly widen the frequency range of the resonance region at the same excitation level.

The measurements were also performed on vibration modes (2,13) with axial load of 2 kN. The results confirmed the nonlinear vibrations behavior previously mentioned [6].

5.4.2 Nonlinear Vibrations of Axially Imperfect Shells

Basic Behavior

The behavior of the nonlinear vibrations of shell Liuip01 and Liuip02 are qualitatively the same as those of the perfect shell. Theoretically the influence of the imperfections is marked by the disappearance of the coupled mode response at

Note: In Fig.12 during the downward sweep at freq. lower than 508 Hz some malfunctions of the measurement system occurred and no data were recorded. From observation, the response was in the form of beating which then at amplitude of about 1.2 times wall thickness jumped to lower branch.

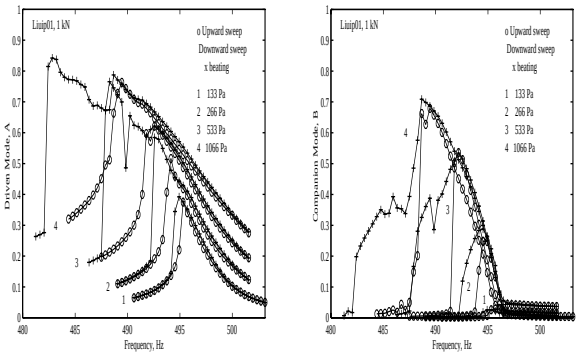

Figure 14 Response of shell Liuip01 with 1 kN axial load

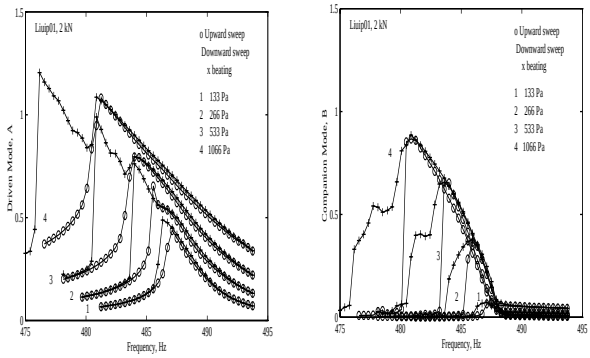

Figure 15 Response of shell Liuip01 with 2 kN axial load

low frequencies [9]. In the experiment this was observed as well. The results for the imperfect shells are shown in Figs.14 to 17 for shell Liuip01. The type of nonlinearity at a response level of 1.5 times wall thickness is of a softening type, as expected.

Influence of Excitation Level and Axial Load

The axisymmetric imperfections do not change the behavior of the response of shells at different excitation level and axial load. Higher response levels widen the frequency range of the coupled mode response of which the upper frequency limit does not shift. They also cause the jump phenomenon and the peak of the coupled mode response to become more pronounced. The axial load lowers the natural frequency.

5.4.3 Measurement of Contractive Motion

In a few cases, the contractive motion which plays an important role in the nonlinear vibration characteristics of the shell was measured. A result which indicated the motion was measured. It was, however, less convincing as it might be interfered with the distortion of the excitation force and the nonlinearity of the transducer [6].

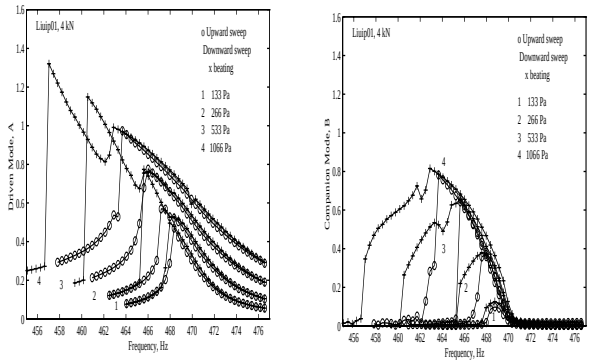

Figure 16 Response of shell Liuip01 with 4 kN axial load

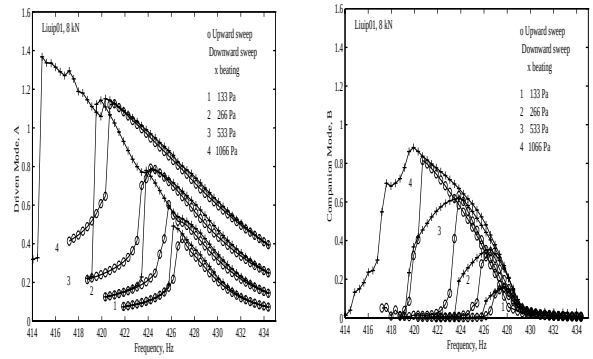

Figure 17 Response of shell Liuip01 with 8 kN axial load

6. Comparisons with Calculated Results

6.1 Validation of Numerical Methods

To validate the theoretical analyses at large amplitudes and various conditions of excitation level, axial load and axisymmetric imperfection, the criteria used are:

1. The freq. range of the companion mode
2. The shape of the driven and the companion mode responses
3. The presence of nonstationary responses.

The calculated response of shell Liupf01 with simply supported boundary conditions is shown in Fig.18. The excitation level corresponded to a sound pressure of 1066 Pa, the axial load was 2 kN and the damping level was determined from the measured damping at low response level (ζ=0.2%). The companion mode appears in a frequency range centered at the natural frequency of the shell with amplitudes comparable to those of the driven mode. In a small region, between 496 Hz and 497 Hz, a modulated coupled mode response occurs, similar to the response shown in Fig.7.c. For comparison, the measured response of shell

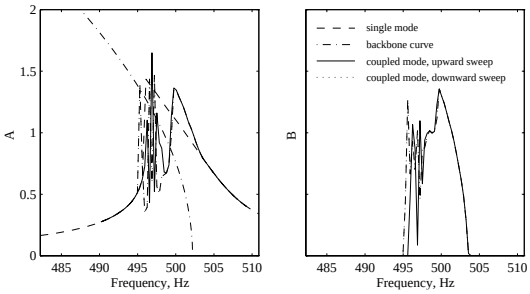

Figure 18 Calculated response of shell Liupf01 with an axial load of 2 kN and an excitation force equal to sound pressure of 1066 Pa

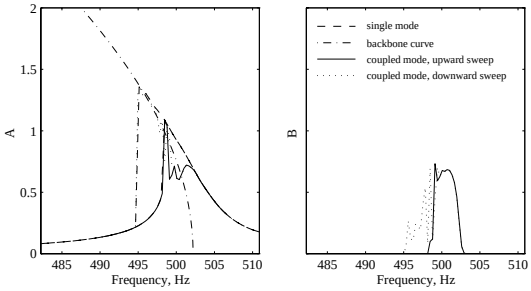

Figure 19 Response of shell Liupf01 with an axial load of 2 kN and an excitation force equal to sound pressure of 533 Pa

Liupf01 at the same axial load and excitation force can be found in Fig.11 for clamped-clamped boundary conditions. Both figures show some quantitative differences, namely the natural frequency and the response level. The difference in natural frequency is attributed to the different boundary conditions of the shells in the experiment and analysis.

Qualitative agreement between the measured and calculated response exists for the upward frequency sweep response. This also holds for the downward frequency sweep response except for a difference between measurement and calculation existing in the low frequency parts of the response. In the experiment the response of this branch could be measured during the downward frequency sweep, however, this response was only conditionally stable.

By decreasing the excitation frequency through the frequency range where beating responses were observed, a stable coupled mode response was obtained again. By further decreasing the excitation frequency, the coupled mode response became unstable and it jumped down to a single mode response. In the

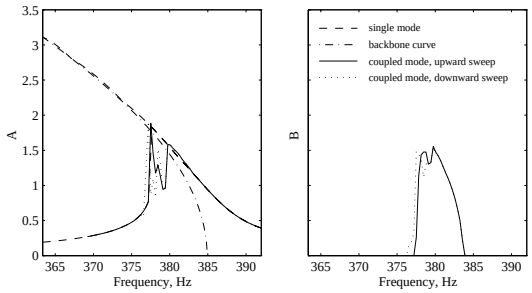

Figure 20 Response of shell Liupf01 with an axial load of 8 kN and an excitation force equal to sound pressure of 1066 Pa

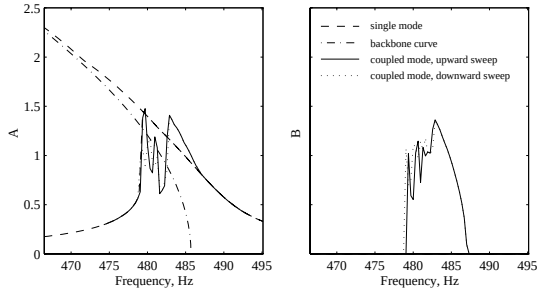

Figure 21 Response of shell Liuip01 with an axial load of 2 kN and an excitation force equal to sound pressure of 1066 Pa, with imperfection neglected

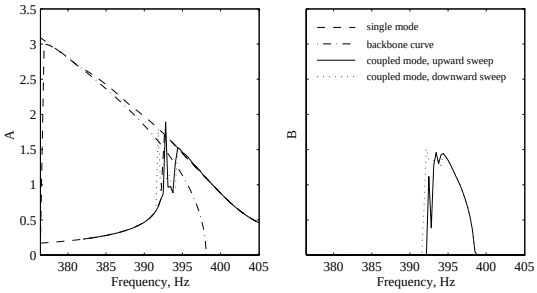

Figure 22 Response of shell Liuip01 with an axial load of 2 kN and an excitation force equal to sound pressure of 1066 Pa and an imperfection with amplitude δ_1=–0.35

calculation, as soon as the excitation frequency reached a frequency at which a stable single mode response was possible, the beating response jumped to that stable response. The branch of the stable coupled mode response at the left side of the beating frequency range was never obtained by numerical simulation method.

6.1.1 Influence of Excitation Level

The influence of excitation level can be seen by comparing Fig.18 and 19. An increase of excitation level increases the response level and widens the frequency range of the coupled mode response. The wider frequency range is caused

primarily by the lower frequency boundary, whereas the higher frequency boundary stays more or less the same. The increased excitation force makes the coupled mode response peak also sharper. The experimental results shown in Fig.10 to 17, in particular Fig.11 for an almost identical case, reveal similar characteristics.

6.1.2 Influence of Axial Load

An increase of the axial load reduces the natural frequency and only slightly increases the response level. This can be seen by comparing Fig.18 and 20 in which the response of shell Liupf01 was calculated for an axial load of 8 kN. The frequency range of the coupled mode response shifts to lower frequencies with the right frequency boundary near its resonant frequency. In the experiment, these phenomena are observed as well by comparing Fig.11 to Fig.13.

6.1.3 Influence of Axisymmetric Imperfection

The influence of axisymmetric imperfections can be observed by comparing Figs.21 and 22 in which the response of mode (1,9) of shell Liuip01 was calculated for two conditions, with and without an axial imperfection, respectively. The amplitude of the axisymmetric imperfection was δ_1=–0.35 (Eq.6), the axial load is 2 kN, and the excitation level 1066 Pa. The axisymmetric imperfection slightly reduces the natural frequency and shifts the frequency range of the coupled mode response accordingly, but it does not change the characteristics of the response of a perfect shell. In the experiment, this can be seen by comparing the response shown in Fig.15 with the responses of the perfect shells presented in Fig.11.

7. Conclusions

A good qualitative agreement between the experiment and the numerical integration method was observed in the experimental validation of the analysis of nonlinear vibration of thin walled cylindrical shells.

The theoretically predicted characteristics of nonlinear vibrations of the thin-walled cylindrical shells at large amplitudes, i.e. the softening nonlinearity and response in the form of traveling waves in the frequency range around the resonance were measured in the experiments.

The influence of several parameters, such as the axisymmetric imperfection, excitation level, frequency sweep direction and axial load were also validated.

8. References

[1] Evensen, DA. *A Theoretical and Experimental Study of Nonlinear Flexural Vibrations of Thin Circular Rings*. NASA TR R-227, 1965.

[2] Gunawan, L, Klompe, AWH and Zwaan, R. *Nonlinear vibration tests of isotropic cylindrical shells under compressive axial loads*, In 20th ICAS Proceedings pp.2434-2444, Sorrento, Italy, 1996.

[3] Gunawan, L and Jansen, EL. *Nonlinear vibrations of cylindrical shells under compressive axial loading.* In Conference on Spacecraft Structures, Materials & Mechanical Testing, pp.707-714, Noordwijk, The Netherlands, 1996.

[4] Gunawan, L. *Imperfection measurement of a perfect shell with specially designed equipment (UNIVIMP).* Report LR-807, Faculty of Aerospace Engineering, Delft University of Technology, The Netherlands, 1996.

[5] Gunawan, L. *Imperfection measurement of shell liupf02, liuip01 and liuip02*. Memorandum M-800, Faculty of Aerospace Engineering, Delft University of Technology, 1997.

[6] Gunawan, L. *Experimental study of nonlinear vibrations of thin-walled cylindrical shells.* Doctoral Thesis, Faculty of Aerospace Engineering, Delft University of Technology, The Netherlands, 1998.

[7] Jansen, E.L. *Nonlinear vibrations of composite cylindrical shells.* Doctoral Thesis, Faculty of Aerospace Engineering, Delft University of Technology, The Netherlands, 1988.

[8] Liu, D.K. *Survey and suggestions for experiments of nonlinear vibrations of thin-walled cylindrical shells.* Report LR-458, Faculty of Aerospace Engineering, Delft University of Technology, The Netherlands, 1985.

[9] Liu, D.K. *Nonlinear vibration characteristics of imperfect shells under compressive axial loads.* Doctoral Thesis, Faculty of Aerospace Engineering, Delft University of Technology, The Netherlands, 1988.

[10] Leissa, A.W. *Vibration of shells.* NASA SP-288, Washington DC, 1973.

[11] Soedel, W. *Vibrations of shells and plates.* Marcel Dekker Inc., 2nd ed., 1993

[12] Tsuei, YG, Shen, ,CL and Liu, J. *Inextensional modes of circular cylinder*. Proceedings of 5th IMAC, pp.869-902, London,1987.